AIP | The Journal of Chemical Physics

# On the way to the highest coordination number in the planar metal-centred aromatic Ta©B10 cluster: Evolution of the structures of TaB n (n = 3–8)

Wei-Li Li, Alexander S. Ivanov, Jozef Federi, Constantin Romanescu, Ivan ernušák, Alexander I. Boldyrev, and Lai-Sheng Wang

Citation: The Journal of Chemical Physics **139**, 104312 (2013); doi: 10.1063/1.4820401
View online: http://dx.doi.org/10.1063/1.4820401
View Table of Contents: http://scitation.aip.org/content/aip/journal/jcp/139/10?ver=pdfcov
Published by the AIP Publishing

**Articles you may be interested in**

Benzene analogues of (quasi-)planar M@B n H n compounds (M = V, Cr, Mn+): A theoretical investigation
J. Chem. Phys. **139**, 174310 (2013); 10.1063/1.4827517

A combined photoelectron spectroscopy and ab initio study of the quasi-planar B24 cluster
J. Chem. Phys. **139**, 144307 (2013); 10.1063/1.4824156

Photoelectron spectroscopy of boron-gold alloy clusters and boron boronyl clusters: B3Au n and B3(BO) n (n = 1, 2)
J. Chem. Phys. **139**, 044308 (2013); 10.1063/1.4816010

On the structures and bonding in boron-gold alloy clusters: B6Au n and B6Au n (n = 13)
J. Chem. Phys. **138**, 084306 (2013); 10.1063/1.4792501

Probing the structures and chemical bonding of boron-boronyl clusters using photoelectron spectroscopy and computational chemistry: B4(BO) n (n = 1–3)
J. Chem. Phys. **137**, 044307 (2012); 10.1063/1.4737863

AIP Publishing Re-register for Table of Content Alerts

Create a profile. Sign up today!

This article is copyrighted as indicated in the article. Reuse of AIP content is subject to the terms at: http://scitation.aip.org/termsconditions. Downloaded to IP: 128.148.231.12 On: Mon, 26 May 2014 19:59:40

THE JOURNAL OF CHEMICAL PHYSICS **139**, 104312 (2013)

# On the way to the highest coordination number in the planar metal-centred aromatic Ta©$B_{10}^-$ cluster: Evolution of the structures of $TaB_n^-$ ($n$ = 3–8)

Wei-Li Li,[1] Alexander S. Ivanov,[2] Jozef Federič,[3] Constantin Romanescu,[1] Ivan Černušák,[3,a)] Alexander I. Boldyrev,[2,b)] and Lai-Sheng Wang[1,c)]
[1]*Department of Chemistry, Brown University, Providence, Rhode Island 02912, USA*
[2]*Department of Chemistry and Biochemistry, Utah State University, 0300 Old Main Hill, Logan, Utah 84322-0300, USA*
[3]*Department of Physical and Theoretical Chemistry, Faculty of Natural Sciences, Comenius University, Mlynská dolina CH1, 84215 Bratislava, Slovakia*

(Received 18 July 2013; accepted 22 August 2013; published online 12 September 2013)

The structures and chemical bonding of $TaB_n^-$ ($n$ = 3–8) clusters are investigated systematically to elucidate the formation of the planar metal-centred aromatic borometallic cluster, Ta©$B_{10}^-$ (the © sign is used to designate the central position of the doped atom in monocyclic structures in M©$B_n$-type planar clusters), which was found previously to have the highest coordination number for a metal atom in a planar geometry. Photoelectron spectroscopy is combined with *ab initio* calculations to determine the global minima of the $TaB_n^-$ clusters. We find that from $TaB_3^-$ to $TaB_5^-$ the boron atoms nucleate around the central Ta atom to form fan-like structures. A structural transition occurs at $TaB_6^-$, which is found to have a hexagonal structure, but with a boron atom in the centre and the Ta atom on the periphery. $TaB_7^-$ is shown to have a three-dimensional boat-like structure, which can be viewed as a Ta atom coordinated to an elongated $B_7$ cluster from above. The global minimum of the $TaB_8^-$ cluster is found to be pyramidal with the Ta atom interacting with a $B_8$ monocyclic ring. Starting from this structure, additional boron atoms simply enlarge the boron ring to form the slightly pyramidal $TaB_9^-$ cluster and eventually the perfectly planar Ta-centred $B_{10}$-ring aromatic cluster, Ta©$B_{10}^-$. It is shown that boron atoms do not nucleate smoothly around a Ta atom on the way to the decacoordinated Ta©$B_{10}^-$ molecular wheel, but rather the competition between B–B interactions and Ta–B interactions determines the most stable structures of the smaller $TaB_n^-$ ($n$ = 3–8) clusters. © *2013 AIP Publishing LLC*. [http://dx.doi.org/10.1063/1.4820401]

## I. INTRODUCTION

As a second-row element, boron has some unique properties that differentiate it from its neighbours in Group 13 and from the rest of the metalloids in the Periodic Table. The peculiar features of boron chemistry can be attributed to its electron deficiency (four valence atomic orbitals with only three valence electrons). Owing to this electron configuration ($2s^2 2p^1$), boron favours multi-centre bonds with pairs of electrons shared among three or more atoms, resulting in interesting three-dimensional (3D) cage structures in bulk boron and boranes. However, joint photoelectron spectroscopy (PES) and computational studies over the past decade have shown that bare boron clusters ($B_n$) are planar or quasi-planar at least up to $n$ = 23 for anions.[1–12] Neutral boron clusters become 3D at $B_{20}$,[7] which have been reaffirmed by recent computational studies.[13,14] Positively charged boron clusters have been shown to become 3D at $B_{16}^+$.[15] Small planar boron clusters starting from $n$ = 7 are composed of a periphery featuring strong covalent two-centre two-electron (2c-2e) B–B $\sigma$-bonds and one or more inner atoms, which interact with the periphery through delocalized $\sigma$ and $\pi$ bonding.[16] Two anionic clusters $B_8^{2-}$ ($D_{7h}$) and $B_9^-$ ($D_{8h}$) were found to be perfectly symmetric and doubly ($\pi$ and $\sigma$) aromatic molecular wheels with a central B atom.[2,17] Chemical bonding analyses revealed that in both clusters each B atom in the periphery contributes two electrons to the B–B peripheral covalent bonds and one electron to the delocalized bonds, whereas the central B atom contributes all its valence electrons to the delocalized bonds.[18–20] An intriguing question arose: is it possible to substitute the central boron atom in the $B_8^{2-}$ and $B_9^-$ molecular wheels with a heteroatom, thus creating highly coordinated monocyclic boron clusters? $CB_6^{2-}$ and $CB_7^-$ were proposed computationally to form carbon-centred molecular wheels.[21,22] However, the reported high-symmetry $CB_6^{2-}$ and $CB_7^-$ structures were only local minima, as confirmed by joint experimental and theoretical studies that the carbon atom (being more electronegative than boron) avoids hyper-coordination in binary $B_xC_y$ clusters.[20,23–25] Subsequent computational studies on silicon-centred clusters suggested that planar structures could be obtained by consecutively adding B atoms to the periphery of a Si-centred $C_{2v}$-$B_nSi_2Si^-$ molecular fan.[26] A perfect planar octacoordinated-Si is achieved at $B_8Si$ ($D_{8h}$).[22,27] These examples indicate the plausibility of nonmetal-centred monocyclic boron clusters, albeit none has been experimentally confirmed. Some attention has been turned to replacing the central boron atom with a metal atom. We have shown previously that valence isoelectronic substitution of the central boron atom by

a)Electronic mail: cernusak@fns.uniba.sk.
b)Electronic mail: a.i.boldyrev@usu.edu.
c)Electronic mail: Lai-Sheng_Wang@brown.edu.

 © 2013 AIP Publishing LLC

This article is copyrighted as indicated in the article. Reuse of AIP content is subject to the terms at: http://scitation.aip.org/termsconditions. Downloaded to IP: 128.148.231.12 On: Mon, 26 May 2014 19:59:40

aluminium in $B_8^{2-}$ and $B_9^-$ led to umbrella-type structures for $AlB_7^-$ ($C_{6v}$) and $AlB_8^-$ ($C_{7v}$),[28] in which the Al atom forms ionic bonds within a quasi-planar $B_7^{3-}$ or $B_8^{2-}$ moiety and does not participate in delocalized bonding. Formation of ionic bonds in Al-doped boron clusters was also observed for larger $AlB_n^-$ ($n = 9$–11) clusters.[29,30] Hence, it appears unlikely that main group atoms are capable of forming molecular wheels with boron rings other than the boron atom itself.

A number of computational studies have examined the possibility of substituting the central B atom in $B_8^{2-}$ and $B_9^-$ by a transition metal atom.[31] Recently, we have experimentally and theoretically characterized the first transition metal centred boron wheels,[32] which led to the proposal of a design principle based on $\pi$ and $\sigma$ double aromaticity and the "ⓒ" symbol to designate the structures of this type of molecular wheels.[33] The design principle, derived from the bonding model of the doubly aromatic $B_8^{2-}$ (BⓒB$_7^{2-}$) and $B_9^-$ (BⓒB$_8^-$) clusters,[2] requires that, in order to form a stable M-centred M$^{(x)}$ⓒB$_n^{q-}$ molecular wheel, the bonding electrons in the system ($3n + x + q$) participate in $n$ 2c-2e B–B peripheral bonds and two sets of aromatic delocalized bonds ($\pi$ and $\sigma$), each fulfilling the Hückel's rule for aromaticity ($4N + 2$ electrons), where $n$ is the number of peripheral boron atoms, $x$ is the formal valence of the transition metal, $q$ is the cluster's charge, and $N$ is an integer. Stable planar molecular wheels of this type that fill the design principle and that have been characterized both experimentally and theoretically thus far include: FeⓒB$_8^-$ and FeⓒB$_9^-$,[34] CoⓒB$_8^-$ and RuⓒB$_9^-$,[32] TaⓒB$_{10}^-$ and NbⓒB$_{10}^-$,[35] and RhⓒB$_9$ and IrⓒB$_9$.[36] In addition to the electronic requirement, we have found that the geometric fitness is also essential. For instance, in a recent study we showed that even though the $VB_{10}^-$ system fulfils the electronic requirement to form a $D_{10h}$-VⓒB$_{10}^-$ aromatic molecular wheel, the V atom is too small to stabilize the ten-membered boron ring.[37] On the other hand, the $B_9$ ring fits well a V atom to form a perfectly planar VⓒB$_9^{2-}$ wheel, whereas it is too small to fit a Nb or Ta atom.[38] Global minimum searches for planar boron wheels with a central hypercoordinate atom (MⓒB$_n$, where M is a second or third row element) revealed that most of the boron wheels are only local minima.[39] Among the experimentally characterized MⓒB$_n^-$ wheels, the TaⓒB$_{10}^-$ and NbⓒB$_{10}^-$ clusters represent the highest coordination number achieved for planar systems.[35,40] It would be interesting to understand atom-by-atom how these remarkable structures are formed. Theoretical calculations on $TiB_n$ ($n = 1$–10) clusters showed that planar two-dimensional (2D) fan- and wheel-type structures are more stable than three-dimensional pyramidal structures.[41] However, the calculations were done at relatively low level of theory and whether these structures are true global minima on their potential energy surfaces was not addressed. Furthermore, the viability of Ti-containing molecular wheels of any size has not been examined experimentally. Beside a recent study on $Ta_2B_n^-$ ($n = 2$–5),[42] there have been no prior studies of the small $TaB_n^-$ clusters. An interesting question arises, concerning the structures of these precursors to the decacoordinated TaⓒB$_{10}^-$: do the boron atoms nucleate around the Ta atom in fan-like structures on the way to the highest coordinate Ta or are there non-planar structures and structural transitions?

In this article we provide an extensive and systematic experimental and theoretical studies on a series of TaⓒB$_n^-$ ($n = 3$–8) clusters to examine how boron atoms nucleate around the Ta atom to form the highest coordination molecular wheel in TaⓒB$_{10}^-$. We found that in the small TaⓒB$_n^-$ ($n = 3$–5) clusters the B atoms form a fan structure around the Ta atom, as expected. However, the cluster structure takes a different turn at $TaB_6^-$, which has a B-centred hexagonal structure with Ta on the periphery, whereas $TaB_7^-$ has a 3D structure. Only at $TaB_8^-$ is a complete $B_8$ ring formed with a pyramidal structure. From then on, the boron ring enlarges with each additional B atom until the perfect decagonal wheel-type structure is achieved at the TaⓒB$_{10}^-$ ($D_{10h}$) cluster.

## II. EXPERIMENTAL AND COMPUTATIONAL METHODS

### A. Photoelectron spectroscopy method

The experiment was performed using a magnetic-bottle PES apparatus equipped with a laser vaporization cluster source, details of which have been published in Ref. 43. Briefly, the $TaB_n^-$ clusters were produced by laser vaporization of a composite disk target made of ~10% isotopically enriched $^{11}B$ and ~15% Ta balanced by Bi or Ag. The latter acted as a binder and also provided atomic $Bi^-$ or $Ag^-$ anions as calibrants for the PES experiment. The clusters were entrained by a He carrier gas seeded with 5% Ar and underwent a supersonic expansion to form a collimated and cold cluster beam. The negatively charged clusters were analyzed with a time-of-flight mass spectrometer. The species of interest were mass-selected and decelerated before being photodetached by a pulsed laser beam at 193 nm (6.424 eV) from an ArF excimer laser; 266 nm (4.661 eV), 355 nm (3.496 eV), and 532 nm (2.331 eV) from a Nd:YAG laser. Photoelectrons were collected at nearly 100% efficiency by a magnetic bottle and analyzed in a 3.5 m long electron flight tube. The resolution of the apparatus, $\Delta E_k/E_k$, was 2.5%, i.e., ~25 meV for 1 eV electrons.

### B. Global optimization methods

The search for the global minimum structures of $TaB_n^-$ ($n = 3$–8) stoichiometries with different (singlet, doublet, triplet, quartet, quintet, and sextet) electronic states was performed using the Coalescence Kick (CK) program.[10] The CK method subjects large populations of randomly generated structures to a coalescence procedure in which all atoms are pushed gradually to the molecular center of mass to avoid generation of fragmented structures and then optimized to the nearest local minima. These calculations were performed at the PBE0/LANL2DZ[44–46] level of theory. The lowest energy isomers ($\Delta E < 30$ kcal mol$^{-1}$) were then reoptimized at PBE0/Ta/Stuttgart/ B/aug-cc-pVTZ[47–51] and single-point calculations for the selected isomers were performed using the CCSD(T)/Ta/Stuttgart/B/aug-cc-pVTZ level of theory. Theoretical vertical detachment energies (VDEs) were calculated at the ROPBE0/Ta/Stuttgart/B/

This article is copyrighted as indicated in the article. Reuse of AIP content is subject to the terms at: http://scitation.aip.org/termsconditions. Downloaded to IP: 128.148.231.12 On: Mon, 26 May 2014 19:59:40

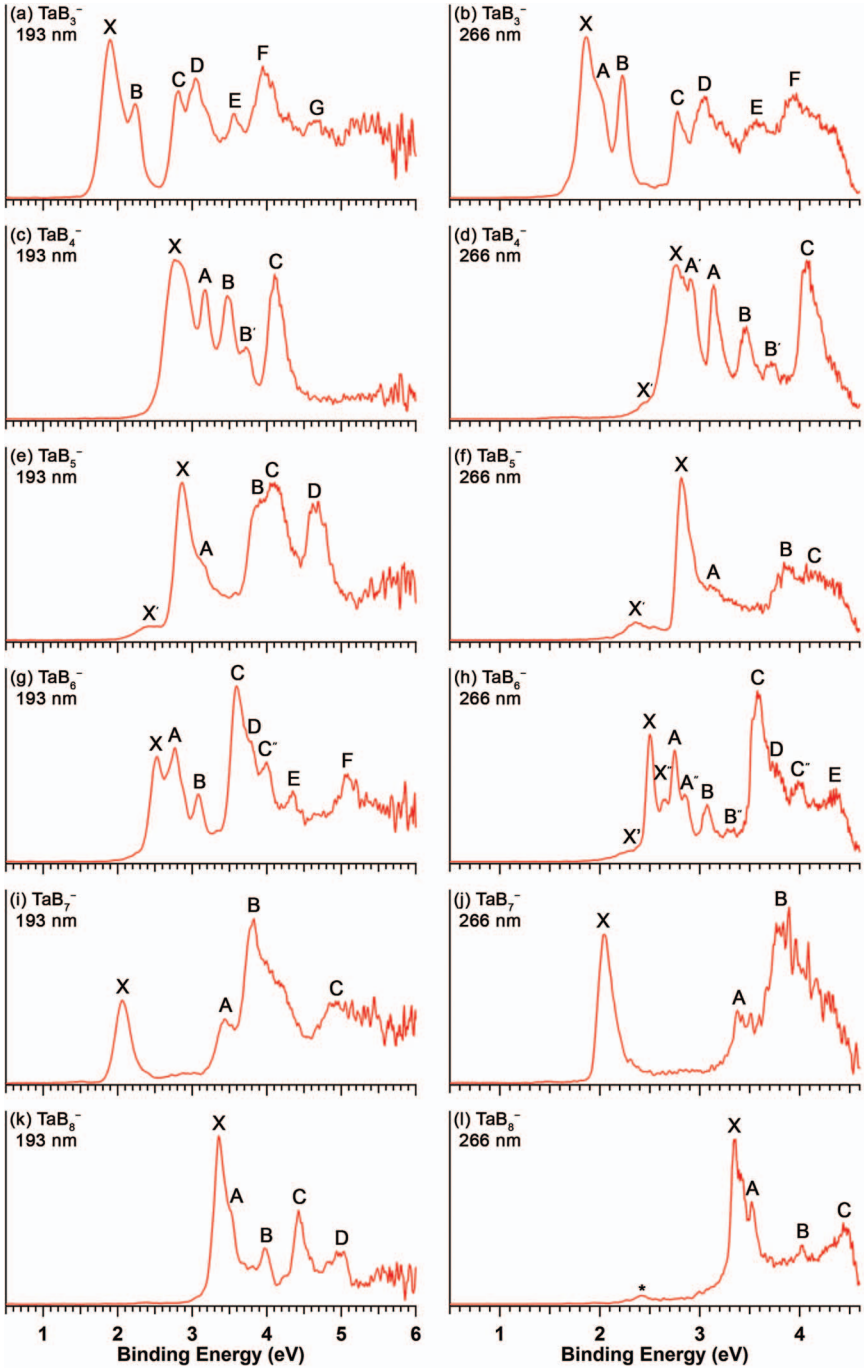


FIG. 1. Photoelectron spectra of $TaB_n^-$ ($n = 3$–8) at 193 nm (left) and 266 nm (right).

aug-cc-pVTZ and ROCCSD(T)/Ta/Stuttgart/B/aug-cc-pVTZ// PBE0/Ta/Stuttgart/B/aug-cc-pVTZ levels of theory. Chemical bonding analyses (PBE0/LANL2DZ) of the global minimum structures were performed using the AdNDP method.[19] All calculations were done using GAUSSIAN 09.[52] Molekel 5.4.0.8 was used for molecular orbitals visualization.[53]

## III. EXPERIMENTAL RESULTS

The photoelectron spectra of $TaB_n^-$ ($n = 3$–8) at 193 and 266 nm are shown in Figure 1. For the smaller clusters, we have also obtained spectra at 355 nm ($n = 3$–7) and 532 nm ($n = 3$), which are given in Figs. S1–S5 in the supplementary material.[54] The observed detachment transitions are labeled by letters. The VDEs for the observed PES bands are compared with the theoretical data in Tables I–VI for $n = 3$–8, respectively. In each spectrum, the X band represents the transition from the anionic to the neutral ground states. The A, B, … bands denote transitions to the first, second, … excited states of the neutral species, etc.

The 193 nm spectrum of $TaB_3^-$ (Figure 1(a)) is relatively congested with at least eight resolved detachment bands (X, A–G). The A band is resolved as a shoulder in the

This article is copyrighted as indicated in the article. Reuse of AIP content is subject to the terms at: http://scitation.aip.org/termsconditions. Downloaded to IP: 128.148.231.12 On: Mon, 26 May 2014 19:59:40

TABLE I. Experimental vertical detachment energies (VDEs) compared with calculated VDEs for the global minimum structure I.1 ($C_{2v}$, $^4B_1$) of $TaB_3^-$. All energies are in eV.

| Feature | VDE (Expt.)[a] | Final state and electronic configuration | VDE (Theoretical) ROPBE1PBE[b] | VDE (Theoretical) ROCCSD(T)[c] |
|---|---|---|---|---|
| | | I.1. $C_{2v}$ ($^4B_1$) | | |
| X | 1.87(3) | $^3A_2$, $\{1a_1^{(2)}1b_2^{(2)}2a_1^{(2)}1b_1^{(2)}3a_1^{(2)}2b_2^{(2)}1a_2^{(1)}3b_2^{(0)}4a_1^{(1)}\}$ | 1.93 | 1.82 |
| A | 2.03(4) | $^3B_1$, $\{1a_1^{(2)}1b_2^{(2)}2a_1^{(2)}1b_1^{(2)}3a_1^{(2)}2b_2^{(2)}1a_2^{(1)}3b_2^{(1)}4a_1^{(0)}\}$ | 2.30 | 2.24 |
| B | 2.22(3) | $^3B_2$, $\{1a_1^{(2)}1b_2^{(2)}2a_1^{(2)}1b_1^{(2)}3a_1^{(2)}2b_2^{(2)}1a_2^{(0)}3b_2^{(1)}4a_1^{(1)}\}$ | 2.38 | 2.24 |
| C | 2.78(5) | $^5A_2$, $\{1a_1^{(2)}1b_2^{(2)}2a_1^{(2)}1b_1^{(2)}3a_1^{(2)}2b_2^{(1)}1a_2^{(1)}3b_2^{(1)}4a_1^{(1)}\}$ | 2.55 | 2.51 |
| D | 3.04(5) | $^5B_1$, $\{1a_1^{(2)}1b_2^{(2)}2a_1^{(2)}1b_1^{(2)}3a_1^{(1)}2b_2^{(2)}1a_2^{(1)}3b_2^{(1)}4a_1^{(1)}\}$ | 2.71 | 3.00 |
| E | 3.56(6) | $^5A_1$, $\{1a_1^{(2)}1b_2^{(2)}2a_1^{(2)}1b_1^{(1)}3a_1^{(2)}2b_2^{(2)}1a_2^{(1)}3b_2^{(1)}4a_1^{(1)}\}$ | 3.26 | 3.42 |
| F | 3.95(6) | $^5B_1$, $\{1a_1^{(2)}1b_2^{(2)}2a_1^{(1)}1b_1^{(2)}3a_1^{(2)}2b_2^{(2)}1a_2^{(1)}3b_2^{(1)}4a_1^{(1)}\}$ | 4.07 | 4.06 |
| G | 4.67(8) | $^5A_2$, $\{1a_1^{(2)}1b_2^{(1)}2a_1^{(2)}1b_1^{(2)}3a_1^{(2)}2b_2^{(2)}1a_2^{(1)}3b_2^{(1)}4a_1^{(1)}\}$ | [d] | 4.64 |

[a]Numbers in parentheses represent the uncertainty in the last digit.
[b]VDEs were calculated at ROPBE1PBE/Ta/Stuttgart/B/aug-cc-pVTZ//PBE1PBE/Ta/Stuttgart/B/aug-cc-pVTZ.
[c]VDEs were calculated at ROCCSD(T)/Ta/Stuttgart/B/aug-cc-pVTZ//PBE1PBE/Ta/Stuttgart/B/aug-cc-pVTZ.
[d]VDE could not be calculated at this level of theory.

TABLE II. Experimentally VDEs compared with calculated VDEs for the II.1 ($C_{2v}$, $^1A_1$) global minimum and the II.2 ($C_s$, $^3A''$) low-lying isomer of $TaB_4^-$. All energies are in eV.

| Feature | VDE (Expt.)[a] | Final state and electronic configuration | VDE (Theoretical) ROPBE1PBE[b] | VDE (Theoretical) ROCCSD(T)[c] |
|---|---|---|---|---|
| | | II.1. $C_{2v}$ ($^1A_1$) | | |
| X | 2.78(3) | $^2B_2$, $\{\ldots 3a_1^{(2)}2b_2^{(2)}1b_1^{(2)}4a_1^{(2)}1a_2^{(2)}3b_2^{(1)}\}$ | 2.67 | 2.66 |
| A | 3.14(3) | $^2A_2$, $\{\ldots 3a_1^{(2)}2b_2^{(2)}1b_1^{(2)}4a_1^{(2)}1a_2^{(1)}3b_2^{(2)}\}$ | 3.01 | 3.09 |
| B | 3.46(3) | $^2A_1$, $\{\ldots 3a_1^{(2)}2b_2^{(2)}1b_1^{(2)}4a_1^{(1)}1a_2^{(2)}3b_2^{(2)}\}$ | 3.53 | 3.49 |
| C | 4.07(3) | $^2B_1$, $\{\ldots 3a_1^{(2)}2b_2^{(2)}1b_1^{(1)}4a_1^{(2)}1a_2^{(2)}3b_2^{(2)}\}$ | 4.09 | 4.21 |
| | | II.2. $C_s$ ($^3A''$) | | |
| X′ | ∼2.5 | $^2A''$, $\{\ldots 3a'^{(2)}4a'^{(2)}5a'^{(2)}2a''^{(2)}3a''^{(2)}4a''^{(1)}6a'^{(0)}\}$ | 2.53 | 2.50 |
| | | $^4A'$, $\{\ldots 3a'^{(2)}4a'^{(2)}5a'^{(2)}2a''^{(2)}3a''^{(1)}4a''^{(1)}6a'^{(1)}\}$ | 2.71 | 2.80 |
| A′ | 2.91(4) | $^2A'$, $\{\ldots 3a'^{(2)}4a'^{(2)}5a'^{(2)}2a''^{(2)}3a''^{(2)}4a''^{(0)}6a'^{(1)}\}$ | 3.00 | 2.82 |
| | | $^4A'$, $\{\ldots 3a'^{(2)}4a'^{(2)}5a'^{(2)}2a''^{(1)}3a''^{(2)}4a''^{(1)}6a'^{(1)}\}$ | 3.25 | [d] |
| B′ | 3.71(4) | $^4A''$, $\{\ldots 3a'^{(2)}4a'^{(2)}5a'^{(1)}2a''^{(2)}3a''^{(2)}4a''^{(1)}6a'^{(1)}\}$ | 3.55 | [d] |
| | | $^4A''$, $\{\ldots 3a'^{(2)}4a'^{(1)}5a'^{(2)}2a''^{(2)}3a''^{(2)}4a''^{(1)}6a'^{(1)}\}$ | 3.87 | 4.09 |

[a]Numbers in parentheses represent the uncertainty in the last digit.
[b]VDEs were calculated at ROPBE1PBE/Ta/Stuttgart/B/aug-cc-pVTZ//PBE1PBE/Ta/Stuttgart/B/aug-cc-pVTZ.
[c]VDEs were calculated at ROCCSD(T)/Ta/Stuttgart/B/aug-cc-pVTZ//PBE1PBE/Ta/Stuttgart/B/aug-cc-pVTZ.
[d]VDE could not be calculated at this level of theory.

TABLE III. Experimental VDEs compared with calculated VDEs for the III.1 ($C_{2v}$, $^2A_1$) global minimum and $C_1$ low-lying isomer of $TaB_5^-$. All energies are in eV.

| Feature | VDE (Expt)[a] | Final state and electronic configuration | VDE (Theoretical) ROPBE1PBE[b] | VDE (Theoretical) ROCCSD(T)[c] |
|---|---|---|---|---|
| | | III.1. $C_{2v}$ ($^2A_1$) | | |
| X | 2.81(3) | $^3B_2$, $\{\ldots 2b_2^{(2)}3a_1^{(2)}1b_1^{(2)}4a_1^{(2)}3b_2^{(1)}1a_2^{(2)}4b_2^{(2)}5a_1^{(1)}\}$ | [d] | 2.81 |
| A | 3.09(5) | $^3B_2$, $\{\ldots 2b_2^{(2)}3a_1^{(2)}1b_1^{(2)}4a_1^{(2)}3b_2^{(2)}1a_2^{(2)}4b_2^{(1)}5a_1^{(1)}\}$ | [d] | 2.86 |
| | | $^1A_1$, $\{\ldots 2b_2^{(2)}3a_1^{(2)}1b_1^{(2)}4a_1^{(2)}3b_2^{(2)}1a_2^{(2)}4b_2^{(2)}5a_1^{(0)}\}$ | 2.84 | 2.89 |
| B | 3.89(8) | $^3A_2$, $\{\ldots 2b_2^{(2)}3a_1^{(2)}1b_1^{(2)}4a_1^{(2)}3b_2^{(2)}1a_2^{(1)}4b_2^{(2)}5a_1^{(1)}\}$ | [d] | 3.69 |
| C | 4.09(8) | $^3A_1$, $\{\ldots 2b_2^{(2)}3a_1^{(2)}1b_1^{(2)}4a_1^{(1)}3b_2^{(2)}1a_2^{(2)}4b_2^{(2)}5a_1^{(1)}\}$ | [d] | 4.12 |
| D | 4.65(5) | $^3B_1$, $\{\ldots 2b_2^{(2)}3a_1^{(2)}1b_1^{(1)}4a_1^{(2)}3b_2^{(2)}1a_2^{(2)}4b_2^{(2)}5a_1^{(1)}\}$ | [d] | 4.49 |
| | | III.2. $C_1$ ($^2A$) | | |
| X′ | ∼2.4 | $^1A$, $\{\ldots 3a^{(2)}4a^{(2)}5a^{(2)}6a^{(2)}7a^{(2)}8a^{(2)}9a^{(2)}10a^{(2)}11a^{(0)}\}$ | 2.20 | 2.35 |
| | | $^3A$, $\{\ldots 3a^{(2)}4a^{(2)}5a^{(2)}6a^{(2)}7a^{(2)}8a^{(2)}9a^{(2)}10a^{(1)}11a^{(1)}\}$ | [d] | 2.82 |

[a]Numbers in parentheses represent the uncertainty in the last digit.
[b]VDEs were calculated at ROPBE1PBE/Ta/Stuttgart/B/aug-cc-pVTZ//PBE1PBE/Ta/Stuttgart/B/aug-cc-pVTZ.
[c]VDEs were calculated at ROCCSD(T)/Ta/Stuttgart/B/aug-cc-pVTZ//PBE1PBE/Ta/Stuttgart/B/aug-cc-pVTZ.
[d]VDE could not be calculated at this level of theory.

This article is copyrighted as indicated in the article. Reuse of AIP content is subject to the terms at: http://scitation.aip.org/termsconditions. Downloaded to IP: 128.148.231.12 On: Mon, 26 May 2014 19:59:40

TABLE IV. Experimental VDEs compared with calculated VDEs for the IV.1 ($C_{2v}$, $^3A_2$) global minimum, and IV.2 ($C_{2v}$, $^1A_1$) and IV.3 ($C_{2v}$, $^1A_1$) low-lying isomers of $TaB_6^-$. All energies are in eV.

| Feature | VDE (Expt.)[a] | Final state and electronic configuration | VDE (Theoretical) ROPBE1PBE[b] | VDE (Theoretical) ROCCSD(T)[c] |
|---|---|---|---|---|
| | | IV.1. $C_{2v}$ ($^3A_2$) | | |
| X | 2.49(3) | $^2B_1$, $\{\ldots 1b_1^{(2)}3b_2^{(2)}5a_1^{(2)}4b_2^{(2)}1a_2^{(2)}2b_1^{(1)}5b_2^{(0)}\}$ | [d] | 2.43 |
| A | 2.75(5) | $^2B_2$, $\{\ldots 1b_1^{(2)}3b_2^{(2)}5a_1^{(2)}4b_2^{(2)}1a_2^{(2)}2b_1^{(0)}5b_2^{(1)}\}$ | 2.86 | 2.81 |
| B | 3.07(4) | $^4A_1$, $\{\ldots 1b_1^{(2)}3b_2^{(2)}5a_1^{(2)}4b_2^{(2)}1a_2^{(1)}2b_1^{(1)}5b_2^{(1)}\}$ | 2.80 | 2.99 |
| C | 3.58(3) | $^4B_1$, $\{\ldots 1b_1^{(2)}3b_2^{(2)}5a_1^{(2)}4b_2^{(1)}1a_2^{(2)}2b_1^{(1)}5b_2^{(1)}\}$ | 3.55 | 3.56 |
| D | 3.77(5) | $^4A_2$, $\{\ldots 1b_1^{(2)}3b_2^{(2)}5a_1^{(1)}4b_2^{(2)}1a_2^{(2)}2b_1^{(1)}5b_2^{(1)}\}$ | 3.71 | 3.76 |
| E | 4.36(5) | $^4B_1$, $\{\ldots 1b_1^{(2)}3b_2^{(1)}5a_1^{(2)}4b_2^{(2)}1a_2^{(2)}2b_1^{(1)}5b_2^{(1)}\}$ | 4.44 | [d] |
| F | 5.08(8) | | [d] | [d] |
| | | IV.2. $C_{2v}$ ($^1A_1$) | | |
| X′ | ∼2.3 | $^2B_2$, $\{\ldots 2b_2^{(2)}4a_1^{(2)}1a_2^{(2)}2b_1^{(2)}5a_1^{(2)}6a_1^{(2)}3b_2^{(1)}\}$ | 2.21 | 2.32 |
| | | $^2A_1$, $\{\ldots 2b_2^{(2)}4a_1^{(2)}1a_2^{(2)}2b_1^{(2)}5a_1^{(2)}6a_1^{(1)}3b_2^{(2)}\}$ | 2.62 | 2.73 |
| | | $^2A_1$, $\{\ldots 2b_2^{(2)}4a_1^{(2)}1a_2^{(2)}2b_1^{(2)}5a_1^{(1)}6a_1^{(2)}3b_2^{(2)}\}$ | 3.20 | 3.23 |
| | | $^2B_1$, $\{\ldots 2b_2^{(2)}4a_1^{(2)}1a_2^{(2)}2b_1^{(1)}5a_1^{(2)}6a_1^{(2)}3b_2^{(2)}\}$ | 4.66 | 4.68 |
| | | $^2A_2$, $\{\ldots 2b_2^{(2)}4a_1^{(2)}1a_2^{(1)}2b_1^{(2)}5a_1^{(2)}6a_1^{(2)}3b_2^{(2)}\}$ | 4.72 | 4.73 |
| | | $^2A_1$, $\{\ldots 2b_2^{(2)}4a_1^{(1)}1a_2^{(2)}2b_1^{(2)}5a_1^{(2)}6a_1^{(2)}3b_2^{(2)}\}$ | 4.83 | 4.85 |
| | | IV.3. $C_{2v}$ ($^1A_1$) | | |
| X″ | 2.64(3) | $^2B_1$, $\{\ldots 4a_1^{(2)}2b_1^{(2)}2b_2^{(2)}5a_1^{(2)}3b_2^{(2)}3b_1^{(1)}\}$ | 2.50 | 2.56 |
| A″ | 2.85(3) | $^2B_2$, $\{\ldots 4a_1^{(2)}2b_1^{(2)}2b_2^{(2)}5a_1^{(2)}3b_2^{(1)}3b_1^{(2)}\}$ | 2.86 | 2.84 |
| B″ | 3.28(4) | $^2A_1$, $\{\ldots 4a_1^{(2)}2b_1^{(2)}2b_2^{(2)}5a_1^{(1)}3b_2^{(2)}3b_1^{(2)}\}$ | 3.13 | 3.28 |
| | | $^2B_2$, $\{\ldots 4a_1^{(2)}2b_1^{(2)}2b_2^{(1)}5a_1^{(2)}3b_2^{(2)}3b_1^{(2)}\}$ | 3.70 | 3.72 |
| C″ | 4.00(5) | $^2B_1$, $\{\ldots 4a_1^{(2)}2b_1^{(1)}2b_2^{(2)}5a_1^{(2)}3b_2^{(2)}3b_1^{(2)}\}$ | 3.99 | 3.90 |
| | | $^2A_1$, $\{\ldots 4a_1^{(1)}2b_1^{(2)}2b_2^{(2)}5a_1^{(2)}3b_2^{(2)}3b_1^{(2)}\}$ | 4.90 | 4.86 |

[a]Numbers in parentheses represent the uncertainty in the last digit.
[b]VDEs were calculated at ROPBE1PBE/Ta/Stuttgart/B/aug-cc-pVTZ//PBE1PBE/Ta/Stuttgart/B/aug-cc-pVTZ.
[c]VDEs were calculated at ROCCSD(T)/Ta/Stuttgart/B/aug-cc-pVTZ//PBE1PBE/Ta/Stuttgart/B/aug-cc-pVTZ.
[d]VDE could not be calculated at this level of theory.

266 nm spectrum (Figure 1(b)). We also obtained the spectra of $TaB_3^-$ at 355 and 532 nm at slightly better resolution (Figure S1). Vibrational fine features are partially resolved at 532 nm for the X band with an average spacing of 670 ± 30 $cm^{-1}$. The VDE of the X band is measured from the 532 nm spectrum to be 1.87 ± 0.03 eV. The VDE of the A band is measured from the 355 nm spectrum as 2.03 ± 0.04 eV (Figure S1b). The VDEs of the remaining spectral bands are measured from the peak maxima and all the VDEs are given in Table I.

The 193 nm spectrum of $TaB_4^-$ (Figure 1(c)) reveals four prominent PES bands (X, A–C). A shoulder (A′) is resolved on the lower energy side of the X band in the 266 nm spectrum (Figure 1(d)), where a low binding energy tail (X′) is also discernible. This tail becomes more recognizable in the 355 nm spectrum (Figure S2). As will be shown later, the X′ tail, the A′ feature, and the weak B′ band are all due to a low-lying isomer of $TaB_4^-$. The VDEs of all the observed features are given in Table II.

The 193 nm spectrum of $TaB_5^-$ (Figure 1(e) shows five PES bands (X, A–D) plus a weak low binding energy tail (X′). The A band is relatively weak, while the relative intensities of the B and C bands also decreased significantly at 266 nm (Figure 1(f)). The 355 nm spectrum of $TaB_5^-$ (Figure S3) is

TABLE V. Experimental VDEs compared with calculated VDEs for the V.1 ($C_s$, $^2A'$) global minimum of $TaB_7^-$. All energies are in eV.

| Feature | VDE (Expt.)[a] | Final state and electronic configuration | VDE (Theoretical) ROPBE1PBE[b] | VDE (Theoretical) ROCCSD(T)[c] |
|---|---|---|---|---|
| | | V.1. $C_s$ ($^2A'$) | | |
| X | 2.05(4) | $^1A'$, $\{\ldots 5a'^{(2)}6a'^{(2)}4a''^{(2)}5a''^{(2)}7a'^{(2)}8a'^{(2)}9a'^{(0)}\}$ | 2.09 | 2.18 |
| A | 3.43(8) | $^3A'$, $\{\ldots 5a'^{(2)}6a'^{(2)}4a''^{(2)}5a''^{(2)}7a'^{(2)}8a'^{(1)}9a'^{(1)}\}$ | [d] | 3.32 |
| B | 3.80(8) | $^3A''$, $\{\ldots 5a'^{(2)}6a'^{(2)}4a''^{(2)}7a'^{(2)}5a''^{(1)}8a'^{(2)}9a'^{(1)}\}$ | [d] | 3.91 |
| C | 4.9(1) | | [d] | [d] |

[a]Numbers in parentheses represent the uncertainty in the last digit.
[b]VDEs were calculated at ROPBE1PBE/Ta/Stuttgart/B/aug-cc-pVTZ//PBE1PBE/Ta/Stuttgart/B/aug-cc-pVTZ.
[c]VDEs were calculated at ROCCSD(T)/Ta/Stuttgart/B/aug-cc-pVTZ//PBE1PBE/Ta/Stuttgart/B/aug-cc-pVTZ.
[d]VDE could not be calculated at this level of theory.

This article is copyrighted as indicated in the article. Reuse of AIP content is subject to the terms at: http://scitation.aip.org/termsconditions. Downloaded to IP: 128.148.231.12 On: Mon, 26 May 2014 19:59:40

TABLE VI. Experimental VDEs compared with calculated VDEs for the VI.1 ($C_s$, $^3A''$) global minimum and the VI.2 ($C_{4v}$, $^1A_1$) low-lying isomer of $TaB_8^-$. All energies are in eV.

| Feature | VDE (Expt.)[a] | Final state and electronic configuration | VDE (Theoretical) ROPBE1PBE[b] | VDE (Theoretical) ROCCSD(T)[c] |
|---|---|---|---|---|
| | | VI.1. $C_s$ ($^3A''$) | | |
| X | 3.35 (4) | $^4A'$, $\{\ldots 6a'^{(2)}7a'^{(2)}8a'^{(2)}4a''^{(2)}9a'^{(2)}5a''^{(1)}6a''^{(1)}10a'^{(1)}\}$ | 3.17 | 3.32 |
| | | $^4A''$, $\{\ldots 6a'^{(2)}7a'^{(2)}8a'^{(2)}4a''^{(2)}9a'^{(1)}5a''^{(2)}6a''^{(1)}10a'^{(1)}\}$ | 3.17 | 3.32 |
| A | 3.52 (3) | $^2A''$, $\{\ldots 6a'^{(2)}7a'^{(2)}8a'^{(2)}4a''^{(2)}9a'^{(2)}5a''^{(2)}6a''^{(1)}10a'^{(0)}\}$ | 3.52 | 3.42 |
| | | $^2A'$, $\{\ldots 6a'^{(2)}7a'^{(2)}8a'^{(2)}4a''^{(2)}9a'^{(2)}5a''^{(2)}6a''^{(0)}10a'^{(1)}\}$ | 3.52 | 3.43 |
| B | 3.98 (8) | $^2A''$, $\{\ldots 6a'^{(2)}7a'^{(2)}8a'^{(2)}4a''^{(2)}9a'^{(2)}5a''^{(1)}6a''^{(2)}10a'^{(0)}\}$[d] | 3.84 | 3.78 |
| C | 4.42 (5) | $^4A''$, $\{\ldots 6a'^{(2)}7a'^{(2)}8a'^{(1)}4a''^{(2)}9a'^{(2)}5a''^{(2)}6a''^{(1)}10a'^{(1)}\}$ | 4.23[e] | 4.48[e] |
| D | 5.0 (1) | | [f] | [f] |
| | | VI.2. $C_{4v}$ ($^1A_1$) | | |
| | | $^2B_2$, $\{\ldots 1b_2^{(2)}2e^{(4)}2a_1^{(2)}1a_2^{(2)}3a_1^{(2)}3e^{(4)}4e^{(4)}2b_2^{(1)}\}$ | 3.29 | 3.23 |
| | | $^2E$, $\{\ldots 1b_2^{(2)}2e^{(4)}2a_1^{(2)}1a_2^{(2)}3a_1^{(2)}3e^{(4)}4e^{(3)}2b_2^{(2)}\}$ | 3.43 | 3.52 |
| | | $^2E$, $\{\ldots 1b_2^{(2)}2e^{(4)}2a_1^{(2)}1a_2^{(2)}3a_1^{(2)}3e^{(3)}4e^{(4)}2b_2^{(2)}\}$ | 4.41 | [f] |
| | | $^2A_1$, $\{\ldots 1b_2^{(2)}2e^{(4)}2a_1^{(2)}1a_2^{(2)}3a_1^{(1)}3e^{(4)}4e^{(4)}2b_2^{(2)}\}$ | 5.02 | 5.06 |
| | | $^2A_2$, $\{\ldots 1b_2^{(2)}2e^{(4)}2a_1^{(2)}1a_2^{(1)}3a_1^{(2)}3e^{(4)}4e^{(4)}2b_2^{(2)}\}$ | 5.59 | 5.38 |
| | | $^2A_1$, $\{\ldots 1b_2^{(2)}2e^{(4)}2a_1^{(1)}1a_2^{(2)}3a_1^{(2)}3e^{(4)}4e^{(4)}2b_2^{(2)}\}$ | 6.09 | [f] |

[a]Numbers in parentheses represent the uncertainty in the last digit.
[b]VDEs were calculated at ROPBE1PBE/Ta/Stuttgart/B/aug-cc-pVTZ//PBE1PBE/Ta/Stuttgart/B/aug-cc-pVTZ.
[c]VDEs were calculated at ROCCSD(T)/Ta/Stuttgart/B/aug-cc-pVTZ//PBE1PBE/Ta/Stuttgart/B/aug-cc-pVTZ.
[d]Peak B can only be explained by the shake-up.
[e]VDEs were calculated at UPBE1PBE/Ta/Stuttgart/B/aug-cc-pVTZ and at UCCSD(T)/Ta/Stuttgart/B/aug-cc-pVTZ. The values of $\langle S2 \rangle$ are 3.79 (UPBE1PBE) and 4.11 (UCCSD(T)).
[f]VDE could not be calculated at this level of theory.

not significantly improved. The VDEs of all the observed PES bands are given in Table III.

The 193 nm spectrum of $TaB_6^-$ is quite complicated with many PES transitions (Figure 1(g)). More PES bands (X″, A″, B″) are resolved at 266 nm (Figure 1(h). As will be shown below, there are two low-lying isomers, which can potentially contribute to the observed spectra and result in the congested spectra observed. The VDEs of all the resolved PES bands are given in Table IV.

The 193 nm spectrum of $TaB_7^-$ (Figure 1(i) is relatively simple with four well-resolved bands (X, A–C). Bands B and C are quite broad and may contain multiple electronic transitions. The X band defines a relatively low VDE of 2.05 eV for $TaB_7^-$. The spectra of $TaB_7^-$ suggest that they come from a single stable isomer without any appreciable contribution from low-lying isomers. The observed VDEs for $TaB_7^-$ are given in Table V.

The 193 nm spectrum of $TaB_8^-$ (Figure 1(k) displays five relatively sharp PES bands (X, A–D). The band A is better resolved in the 266 nm spectrum (Figure 1(l), which shows possible vibrational structures for band X. Very weak signals at lower binding energies (labeled as *) are seen in the 266 nm and they may come from a weakly populated isomer. The VDEs of all the observed PES bands for $TaB_8^-$ are given in Table VI.

Overall, the binding energy increases from $TaB_3^-$ to $TaB_5^-$ and then drops at $TaB_6^-$ and reaches a minimum at $TaB_7^-$ before increasing again at $TaB_8^-$. This observation may suggest a structural change at $TaB_6^-$ and $TaB_7^-$. The spectra of $TaB_8^-$ exhibit some similarity to those of $TaB_9^-$ and $TaB_{10}^-$ with systematic increasing VDEs,[35,38] suggesting that $TaB_8^-$ may show structural similarities to the larger Ta©$B_9^-$ and Ta©$B_{10}^-$ molecular wheels.

## IV. THEORETICAL RESULTS

### A. $TaB_3^-$

The unbiased global minimum searches for $TaB_3^-$ in different spin states led to three low energy isomers (Figure 2(a)). The $C_{2v}$ ($^4A_2$) structure I.3 was found to be the lowest energy isomer at the PBE0/Ta/Stuttgart/B/aug-cc-pVTZ level of theory. However, single point calculations at CCSD(T)/Ta/Stuttgart/B/aug-cc-pVTZ and CCSD(T)/Ta/Stuttgart/B/aug-cc-pVQZ for all the low-lying isomers of $TaB_3^-$ (Figure S6) showed that the $C_{2v}$ ($^4B_1$) fan-type structure I.1 is the true global minimum on the potential energy surface of $TaB_3^-$, although isomers I.2 and I.3 are very close in energy to I.1, only 0.2 and 1.6 kcal/mol higher at the CCSD(T)/Ta/Stuttgart/B/aug-cc-pVTZ level of theory.

### B. $TaB_4^-$

Our global minimum search revealed that the fan-like structure (II.1 in Figure 2(b)) is the global minimum for $TaB_4^-$. Single point calculations at CCSD(T)/Ta/Stuttgart/B/aug-cc-pVTZ showed that a similar triplet isomer is only

This article is copyrighted as indicated in the article. Reuse of AIP content is subject to the terms at: http://scitation.aip.org/termsconditions. Downloaded to IP: 128.148.231.12 On: Mon, 26 May 2014 19:59:40

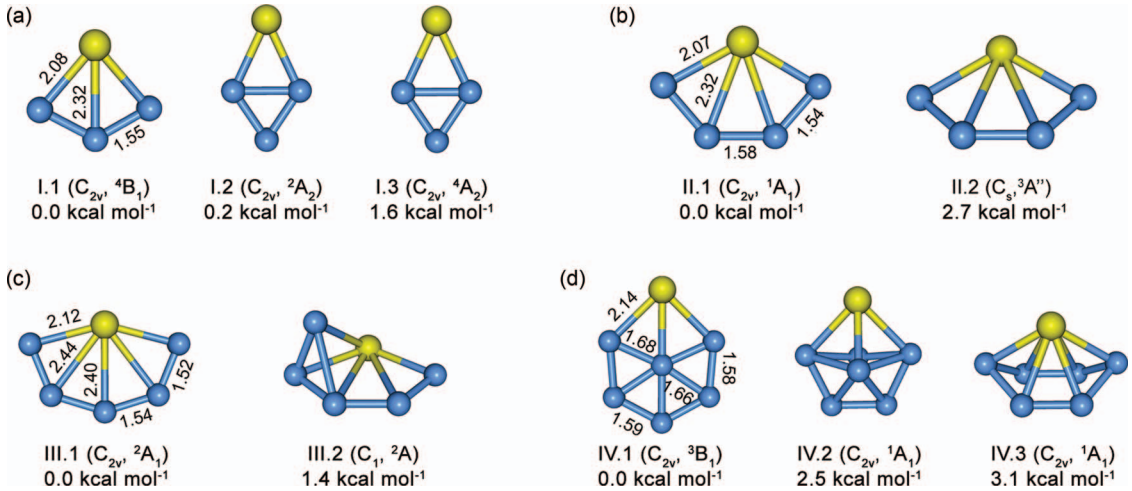


FIG. 2. The global minimum structures and low-lying isomers of (a) $TaB_3^-$, (b) $TaB_4^-$, (c) $TaB_5^-$, and (d) $TaB_6^-$, optimized at the PBE0/Ta/Stuttgart/B/aug-cc-pVTZ level. Also given are the point group symmetries, spectroscopic states, and relative energies at the CCSD(T)/Ta/Stuttgart/B/aug-cc-pVTZ level with ZPE corrections at the PBE0/Ta/Stuttgart/B/aug-cc-pVTZ level. Bond lengths for the global minimum structures are given in Å.

2.7 kcal/mol higher (Figure 2(b), II.2). The II.2 isomer is not completely planar, but the deviation from planarity is very small. A low-symmetry 3D isomer (II.3 in Figure S7) is 8.7 kcal/mol above the global minimum. The global minimum of $TaB_4^-$ continues the fan-like structure observed for $TaB_3^-$.

### C. $TaB_5^-$

The global minimum of $TaB_5^-$ is also a planar fan-like structure (III.1 in Figure 2(c)). The second lowest isomer (III.2 in Figure 2(c)) which is similar to isomer II.3 of $TaB_4^-$ is only 1.4 kcal/mol higher in energy at CCSD(T)/Ta/Stuttgart/B/aug-cc-pVTZ. A more extensive set of alternative isomers found in our global minimum search for $TaB_5^-$ is summarized in Figure S8.

Thus, $TaB_5^-$ continues the fan-growth mode, which is now half way on to the Ta©$B_{10}^-$ molecular wheel. However, some subtle structural trends can be seen from $TaB_3^-$ to $TaB_5^-$: the B−B bond lengths seem to decrease, whereas the Ta−B bond lengths increase. This trend suggests that the interaction between Ta and individual B atoms decreases, while the boron ring motif is taking shape.

### D. $TaB_6^-$

The fan-growth mode is disrupted at $TaB_6^-$. Our global search showed that the most stable structure of $TaB_6^-$ (IV.1 in Figure 2(d)) is planar with a hexagonal shape, but with a B atom in the centre. We also found two boat-like 3D isomers (IV.2 and IV.3 in Figure 2(d)), which are competitive, lying within 3 kcal/mol of isomer IV.1 (CCSD(T)/Ta/Stuttgart/B/aug-cc-pVTZ). The expected fan-shaped structure (IV.5 in Figure S9) is only the fifth lowest isomer of $TaB_6^-$, being 9.8 kcal/mol above IV.1. It seems that the B−B interactions prevail over Ta−B bonding in $TaB_6^-$.

### E. $TaB_7^-$

We found that the global minimum of $TaB_7^-$ is a very stable boat-like 3D structure (Figure 3(a)), which can be viewed as being formed from the IV.3 isomer of $TaB_6^-$. The fan-like structure (V.9 in Figure S10) is now a much higher isomer by 20.2 kcal/mol above the global minimum. Interestingly, the second lowest isomer of $TaB_7^-$ is heptagonal pyramidal structure (V.2 in Figure S10), which is higher than the global minimum by 4.9 kcal/mol (CCSD(T)/Ta/Stuttgart /B/aug-cc-pVTZ). This isomer can be viewed as Ta atom interacting with a $B_7$ ring. Thus, starting from $n = 7$, a boron-ring based

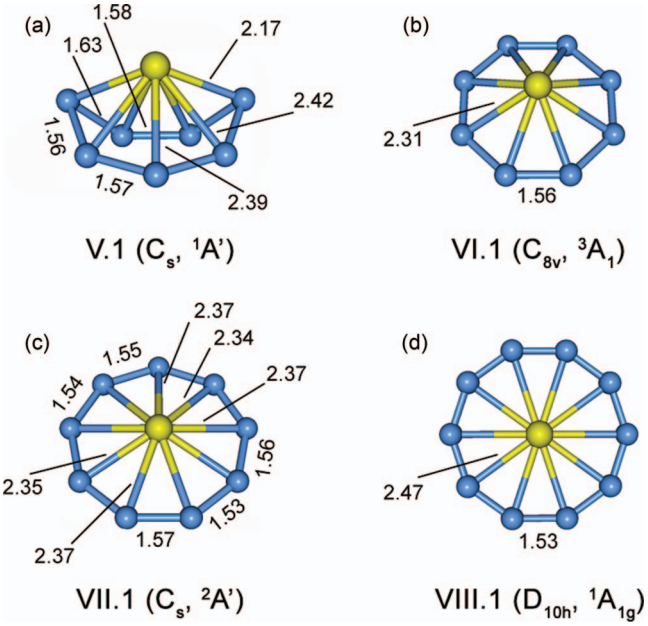


FIG. 3. The global minimum structures of (a) $TaB_7^-$, (b) $TaB_8^-$, (c) $TaB_9^-$, and (d) $TaB_{10}^-$, optimized at PBE0/Ta/Stuttgart/B/aug-cc-pVTZ level. Bond lengths in Å, point group symmetries, and spectroscopic states are also shown. The structures of $TaB_9^-$ and $TaB_{10}^-$, which were reported previously,[35,38] are given for comparison.

This article is copyrighted as indicated in the article. Reuse of AIP content is subject to the terms at: http://scitation.aip.org/termsconditions. Downloaded to IP: 128.148.231.12 On: Mon, 26 May 2014 19:59:40

isomer becomes energetically favorable, even though the global minimum of $TaB_7^-$ is 3D.

### F. $TaB_8^-$

According to our CK search, the global minimum of $TaB_8^-$ is a pyramidal structure with a triplet spin state (Figure 3(b)), in which the Ta atom is interacting with a $B_8$ ring. Ta atom is obviously too large to fit in the centre of the $B_8$ ring to form the planar octacoordinated Ta. Our calculations at the PBE0 level of theory showed that the global minimum VI.1 represents only a low-symmetry $C_s$ structure. However, optimization with follow-up frequency calculations using the exchange-correlation potential PW91PW91[55] and the hybrid meta-exchange-correlation functional M06-2X[56] confirmed the $C_{8v}$ structure VI.1 to be the global minimum. The distortion in the $C_s$ structures relative to the $C_{8v}$ symmetry is small and our chemical bonding analyses yielded very similar results for either $C_s$ or $C_{8v}$ symmetry. The second low-lying isomer is also a pyramidal structure with a singlet spin state and $C_{4v}$ symmetry (VI.2 in Figure S11), in which four boron atoms are slightly pulled out from the molecular framework. The VI.2 isomer is 4.1 kcal/mol higher than the global minimum and all other isomers (Figure S11) are at least 18 kcal/mol higher.

## V. INTERPRETATION OF THE PHOTOELECTRON SPECTRA

### A. $TaB_3^-$

According to the relative energies calculated at the CCSD(T) level, isomer I.1 is the global minimum and should be responsible for the observed PES spectra of $TaB_3^-$. Isomers I.2 and I.3 are quite low-lying (Figure 2(a)) and may be present in the cluster beam and make minor contributions to the PES spectra.

Isomer I.1 is open shell with a quartet ground state ($^4B_1$). The calculated VDEs for $TaB_3^-$ are compared with the experimental data in Table I. Three molecular orbitals are singly occupied in isomers I.1, yielding triplet or quintet neutral final states upon electron detachment. The first VDE corresponds to the electron detachment from the $3b_2$ orbital to produce the $^3A_2$ final state. The calculated VDE of 1.82 eV (all the calculated values discussed in this section are at ROCCSD(T) level of theory) is in excellent agreement with the experimental value of 1.87 ± 0.03 eV. All the other calculated VDEs agree well with the observed major PES bands. There is a small tail in front of peak X at ∼1.6-1.7 eV (Figure S1), which might come from I.2 and I.3. The calculated first VDEs for I.2 and I.3 are 1.64 eV and 1.60 eV, respectively, at the CCSD(T) level of theory. The calculated VDEs for higher energy detachment channels for isomers I.2 and I.3 are given in Table S1. The almost negligible signals in the low binding energy tail in the experimental spectra suggest that the populations of isomers I.2 and I.3 are minor, if at all. Thus, their relative energies may be even higher than the CCSD(T) results indicate.

### B. $TaB_4^-$

The global minimum (II.1) of $TaB_4^-$ is closed shell with a singlet ground state (Figure 2(b)). The triplet isomer II.2 is only 2.7 kcal/mol higher in energy and may be present in the cluster beam and contribute to the photoelectron spectra. The calculated VDE from the $3b_2$ HOMO of II.1 is 2.66 eV (Table II), corresponding to the ground state detachment band X at 2.78 eV. The VDE of the next detachment channel from the $1a_2$ HOMO-1 is calculated to be 3.09 eV, in good agreement with the band A at 3.14 eV. The VDEs from HOMO-2 and HOMO-3 are calculated to be 3.49 eV and 4.21 eV, consistent with the observed bands B (VDE = 3.46 eV) and C (VDE = 4.07 eV), respectively.

Hence, the weak features X′, A′, and B′ must come from the low-lying isomer II.2. This isomer has a triplet ground electronic state, which can yield doublet and quartet final states, as shown in Table II. The first VDE of II.2 is calculated to be 2.50 eV, which agrees well with the weak feature X′ at ∼2.5 eV. The second and third detachment channels were calculated to have very close VDEs of 2.80 and 2.82 eV, which should correspond to the A′ feature. The next two detachment channels could not be calculated at the CCSD(T) level, one of the channels should correspond to the B′ band. The sixth detachment channel with a calculated VDE of 4.09 eV should contribute to the broad C band. Thus, the observed PES spectra can be explained well by isomers II.1 and II.2. Isomer II.2 is a triplet state, which is metastable and cannot relax readily to the singlet ground state in the cluster beam, which is why it was populated even though its energy is relatively high (by 2.7 kcal/mol) above isomer II.1.

### C. $TaB_5^-$

The global minimum isomer III.1 of $TaB_5^-$ (Figure 2(c)) is open shell with a doublet ground electronic state. The first detachment channel is from the fully occupied $3b_2$ MO producing a $^3B_2$ final state (Table III). The calculated first VDE of 2.81 eV is in perfect agreement with the experimental result. The next two detachment channels from the $4b_2$ and $5a_1$ orbitals yielded similar VDEs of 2.86 and 2.89 eV, which should correspond to the broad A band. Following an energy gap, the next three detachment channels yielded VDEs in good agreement with bands B, C, and D in the experiment. The isomer III.2 is only 1.4 kcal/mol above III.1 and is expected to be present in the experiment. Indeed, the calculated first VDE from III.2 of 2.35 eV agrees well with the weak X′ band in the low binding energy side. Higher energy detachment channels are likely buried in the broad features of isomer III.1.

### D. $TaB_6^-$

The global minimum isomer IV.1 of $TaB_6^-$ has a triplet ground state (Figure 2(d)), which can lead to both doublet and quartet final states in PES. The calculated first VDE of 2.43 eV from the $5b_2$ MO is in excellent agreement with band X at 2.49 eV (Table IV). The calculated VDEs for the next four detachment channels at the CCSD(T) level are in excellent agreement with the observed bands A, B, C, and D,

This article is copyrighted as indicated in the article. Reuse of AIP content is subject to the terms at: http://scitation.aip.org/termsconditions. Downloaded to IP: 128.148.231.12 On: Mon, 26 May 2014 19:59:40

respectively. However, higher energy channels corresponding to bands E and F were unfortunately unable to be calculated at CCSD(T). The VDE from PBE at 4.44 eV is in good agreement with band E. These assignments leave several weaker features unaccounted for in the experimental spectra, which must come from low-lying isomers.

Our calculations suggested two 3D isomers (IV.2 and IV.3), which are within 3 kcal/mol of the global minimum (Figure 2(d)). Both are closed shell with singlet spin states and thus are metastable relative to the triplet ground state. They can be populated experimentally, even though their energies are relatively high. The calculated first VDE of isomer IV.2 is 2.32 eV, consistent with the low binding energy tail labeled as X′ in Figure 1(h). The second detachment channel of isomer IV.2 gives a calculated VDE of 2.73 eV, which may contribute to band A, whereas the third detachment channel of isomer IV.2 with a calculated VDE of 3.23 eV could contribute to band B″. The higher detachment channels of isomer IV.2 from 4.68 to 4.85 eV should contribute to the nearly continuous signals in the corresponding spectral range in the 193 nm spectrum (Figure 1(g)).

The calculated VDEs from isomer IV.3 are in excellent agreement with the remaining weak features (X″, A″, B″, C″), as shown in Table IV. The fourth detachment channel of IV.3 at 3.72 eV is likely buried in the intense C band. Overall, the complicated PES spectra of $TaB_6^-$ are well explained by the global minimum and the two 3D low-lying isomers.

### E. $TaB_7^-$

The global minimum 3D structure of $TaB_7^-$ is very stable (Figure 3(a)) and the nearest low-lying isomer is at least 4.9 kcal/mol higher in energy (Figure S10), thus unlikely to be present in the experiment. Indeed, the PES spectra of $TaB_7^-$ are relatively simple with no hint of major low-lying isomer contributions. The first detachment channel from the global minimum V.1 isomer of $TaB_7^-$ is from the 9a′ singlet occupied MO, producing the neutral singlet ground state. The calculated VDE of 2.18 eV is in good agreement with band X at 2.05 eV (Table V). The second detachment channel is from the fully occupied 8a′ orbital with a calculated VDE of 3.32 eV, in excellent agreement with band A at 3.43 eV. The large X-A separation defines a large HOMO-LUMO gap (∼1.4 eV) for the neutral $TaB_7$, suggesting it is a relatively stable cluster. The third detachment is from the 5a″ MO with a calculated VDE of 3.91 eV, in good agreement with the observed band B at 3.80 eV. Even though the VDEs for deeper MOs could not be calculated at these levels of theory, the good agreement between experiment and theory for the first three detachment channels provides strong support for the global minimum of $TaB_7^-$.

### F. $TaB_8^-$

The global minimum of $TaB_8^-$ has a triplet electronic state (either $C_{8v}$ or $C_s$ symmetry). The first and second detachment channels are from the fully occupied 5a″ and 9a′ MOs, producing two quartet final states. The calculated VDEs of 3.32 eV for these detachment channels are the same, in good agreement with band X at 3.35 eV (Table VI). Detachment from the two singly occupied 10a′ and 6a″ MOs, resulting in two doublet final states, also with very similar calculated VDEs, 3.42 and 3.43 eV, respectively, is in good agreement with band A at 3.52 eV. The fifth detachment channel is from the 8a′ MO, producing a quartet final state, with a calculated VDE of 4.48 eV in good agreement with the observed band C at 4.42 eV. The VDEs for higher binding energy MOs could not be calculated at the current level of theory.

However, the above assignment still leaves the lower binding energy B band at 3.98 eV unaccounted for. This feature could be due to contributions from a low lying isomer. The second isomer $TaB_8^-$ is a singlet state, 4.1 kcal/cal above the triplet global minimum (Figure S11). The first calculated VDE for isomer VI.2 is 3.23 eV (Table VI), which is consistent with the very weak tail around 3.2 eV (Figure 1(l)). However, this tail is almost negligible, suggesting that contributions from isomer VI.2 is negligible. Furthermore, there is no detachment channel from isomer VI.2 that agrees with the observed band B. We found that a two-electron detachment channel produced a VDE of 3.78 eV, in good agreement with the observed VDE of band B at 3.98 eV (Table VI). We also note a weak signal around 2.4 eV in the 266 nm spectrum of $TaB_8^-$ (labeled as * in Figure 1(l)). But it is negligible in the 193 nm spectrum (Figure 1(k)). We attributed to it to an unknown impurity.

Overall, the computational results and the experimental data are in good agreement, lending considerable credence to the global minima and the low-lying isomers obtained for all the $TaB_n^-$ ($n = 3$–8) clusters.

## VI. STRUCTURAL EVOLUTION AND CHEMICAL BONDING IN $TaB_n^-$

To understand the structural evolution and how boron atoms nucleate around the central Ta atom to form the highest coordination Ta©$B_{10}^-$ molecular wheel, we analyzed the chemical bonding in $TaB_n^-$ ($n = 3$–8) using the Adaptive Natural Density Partitioning (AdNDP),[19] as shown in Figs. 4–6.

### A. $TaB_n^-$ ($n = 3$–5): Nucleation of B around Ta

The AdNDP analysis for the global minimum $TaB_3^-$ ($C_{2v}$, $^4B_1$) cluster (Figure 4, I.1) revealed four 2c-2e peripheral $\sigma$ bonds (two B–B bonds and two Ta–B bonds) with occupation numbers (ON) ranging from 1.95 |e| to 1.98 |e|, one delocalized 4c-2e $\sigma$ bond and one delocalized 4c-2e $\pi$ bond (ON = 2.00 |e|). Since $TaB_3^-$ has three unpaired electrons, the AdNDP analysis also showed one delocalized 4c-1e $\sigma$ bond (ON = 1.00 |e|), one delocalized 4c-1e $\pi$ bond (ON = 1.00 |e|), and one 1c-1e 6s lone-pair on Ta (ON = 1.00 |e|). The single electron delocalized $\sigma$ and $\pi$ bonds both describe Ta 5*d* bonding with the two terminal B atoms, rendering partial multiple bond characters for the two Ta–B bonds. This bonding picture is consistent with the short terminal Ta–B bond lengths (2.08 Å) and the relatively long bond length between Ta and the central B atom (2.32 Å). The latter is characterized by multicenter delocalized bonding only.

This article is copyrighted as indicated in the article. Reuse of AIP content is subject to the terms at: http://scitation.aip.org/termsconditions. Downloaded to IP: 128.148.231.12 On: Mon, 26 May 2014 19:59:40

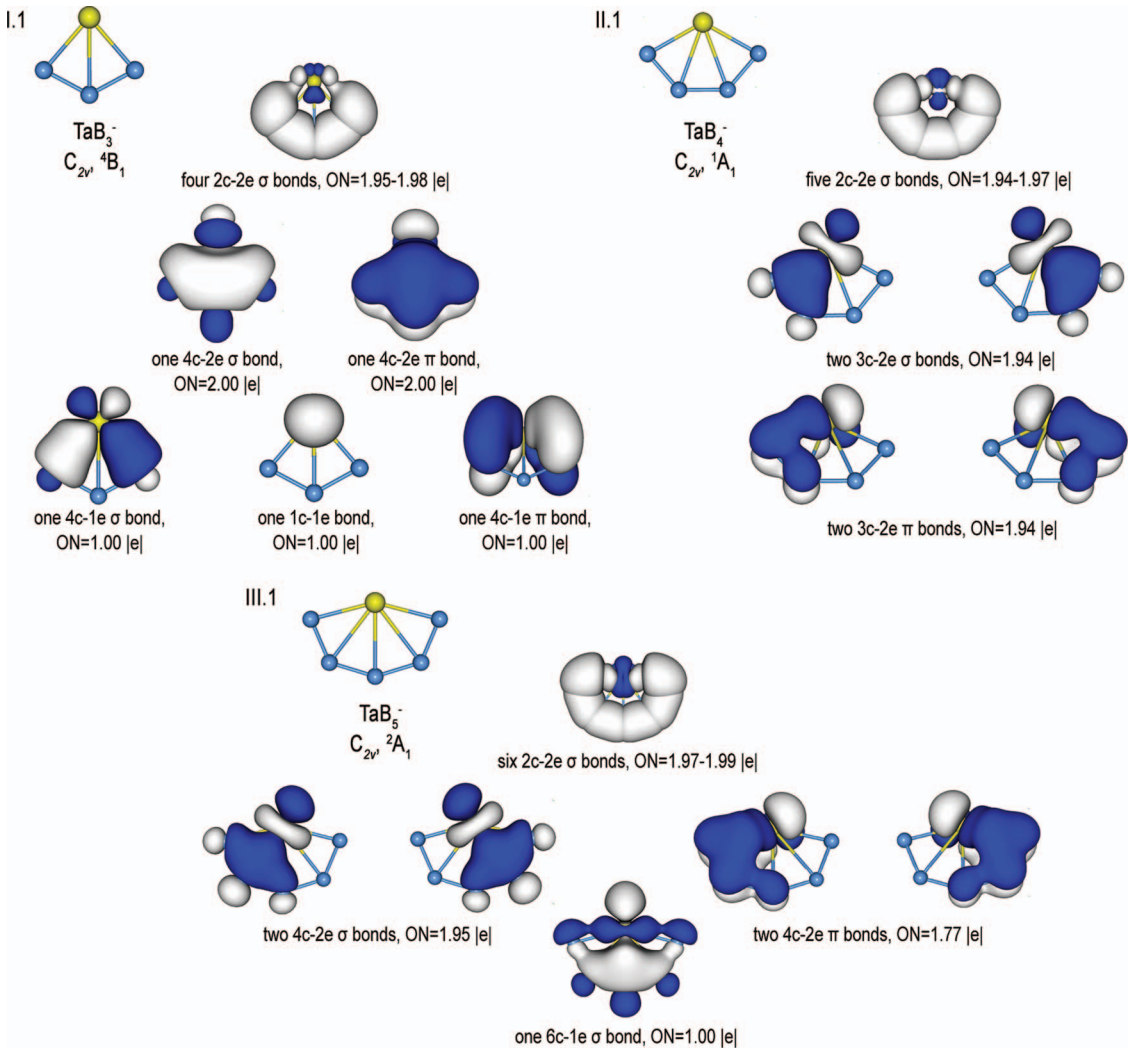


FIG. 4. Results of AdNDP analyses for the global minimum structures of $TaB_3^-$ (I.1), $TaB_4^-$ (II.1), and $TaB_5^-$ (III.1).

The bonding in the global minimum $TaB_4^-$ ($C_{2v}$, $^1A_1$) consists of five localized 2c-2e $\sigma$ peripheral bonds (three B–B bonds and two Ta–B bonds), two delocalized 3c-2e $\sigma$ and $\pi$ bonds (Figure 4, II.1). The two 3c-2e delocalized $\sigma$ bonds describe bonding of Ta with two terminal B–B units, while the two delocalized $\pi$ bonds mainly describe bonding between Ta and the terminal B atoms. Thus, the Ta–$B_{terminal}$ bonds can be viewed as Ta=B double bonds, consistent with the very short Ta–B bond lengths (2.07 Å). From $TaB_3^-$ to $TaB_4^-$, the bonding between Ta and the terminal B atoms is strengthened slightly. Again, the Ta bonding with the two middle B atom is through multicenter delocalized bonding only.

The chemical bonding picture in the $TaB_5^-$ global minimum fan structure is similar to that in $TaB_4^-$. The AdNDP analysis recovered six localized 2c-2e peripheral $\sigma$ bonds (four B–B bonds and two Ta–B bonds), two delocalized 4c-2e $\sigma$ and $\pi$ bonds, and one 6c-1e $\sigma$ bond (ON = 1.00 |e|) (Figure 4, III.1). Thus, the bonds between Ta and the two terminal B atoms contain multiple bond characters, whereas the bonding between Ta and the middle three B atoms is entirely via multicenter delocalized bonding.

### B. $TaB_6^-$ and $TaB_7^-$: Structural excursions

The Ta atom in the global minimum of $TaB_6^-$ ($C_{2v}$, $^3B_1$) is part of a hexagonal ring with a central B atom. Our AdNDP analysis revealed six localized 2c-2e $\sigma$ peripheral bonds for the hexagonal ring, three delocalized 7c-2e $\sigma$ bonds (ON = 2.00 |e|), two 7c-2e $\pi$ bonds (ON = 2.00 |e|), one 1c-1e 5*d* lone-pair (ON = 1.00 |e|), and one delocalized 7c-1e $\pi$ bond (ON = 1.00 |e|) (Figure 5, IV.1). The three delocalized 7c-2e $\sigma$ bonds make $TaB_6^-$ $\sigma$ aromatic. The structure and bonding in $TaB_6^-$ are reminiscent of those in $AlB_6^-$,[30] which has a similar structure with Al being part of the peripheral hexagonal ring and a central B atom. However, the Al atom is slightly out of plane due to $\pi$ antiaromaticity because $AlB_6^-$ only has four delocalized $\pi$ electrons. Clearly, the additional delocalized $\pi$ bond in $TaB_6^-$ is sufficient for a perfect planar structure, even though it only has a single electron. Thus, $TaB_7^-$ can be considered to be doubly aromatic. The $AlB_6^-$ cluster was related to the pyramidal $B_7^-$ cluster and the Al atom was considered as an isoelectronic substitute of a peripheral B atom.[30] The large size of the Al atom enlarges the hexagonal ring and planarizes the central B atom. However,

This article is copyrighted as indicated in the article. Reuse of AIP content is subject to the terms at: http://scitation.aip.org/termsconditions. Downloaded to IP: 128.148.231.12 On: Mon, 26 May 2014 19:59:40

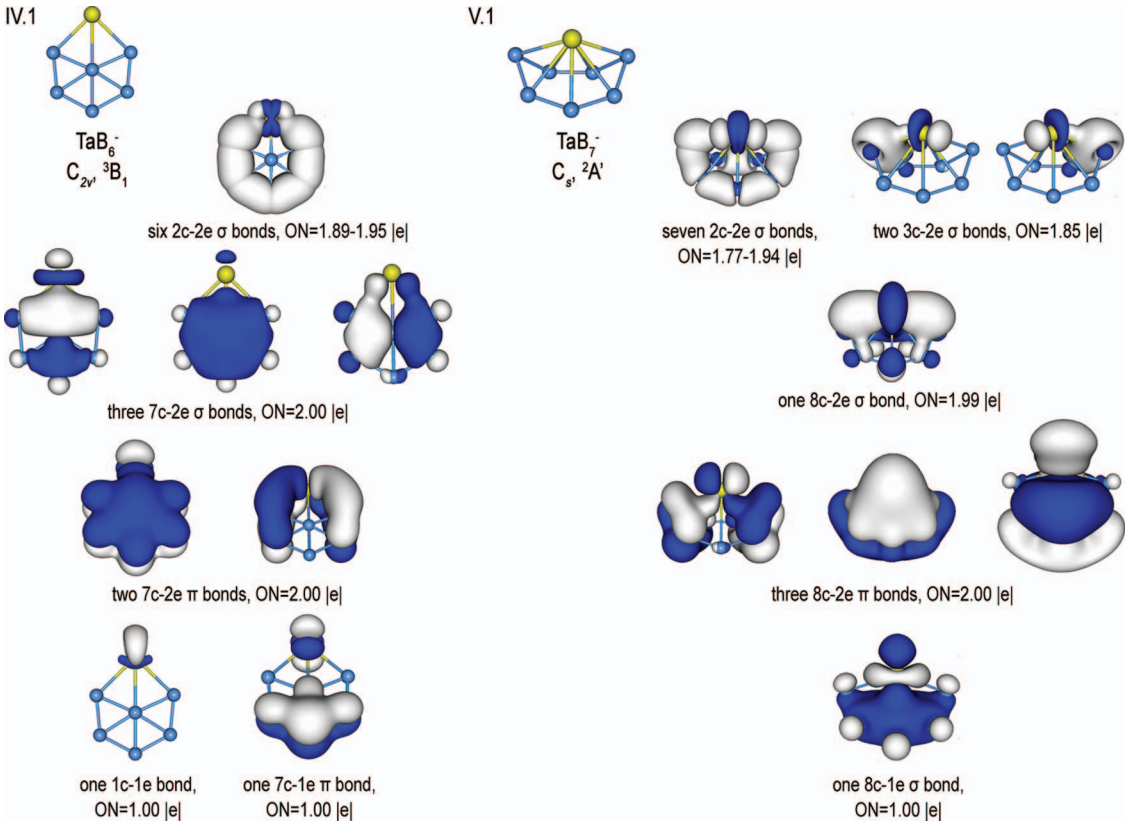


FIG. 5. Results of AdNDP analyses for the global minimum structures of $TaB_6^-$ (IV.1) and $TaB_7^-$ (V.1).

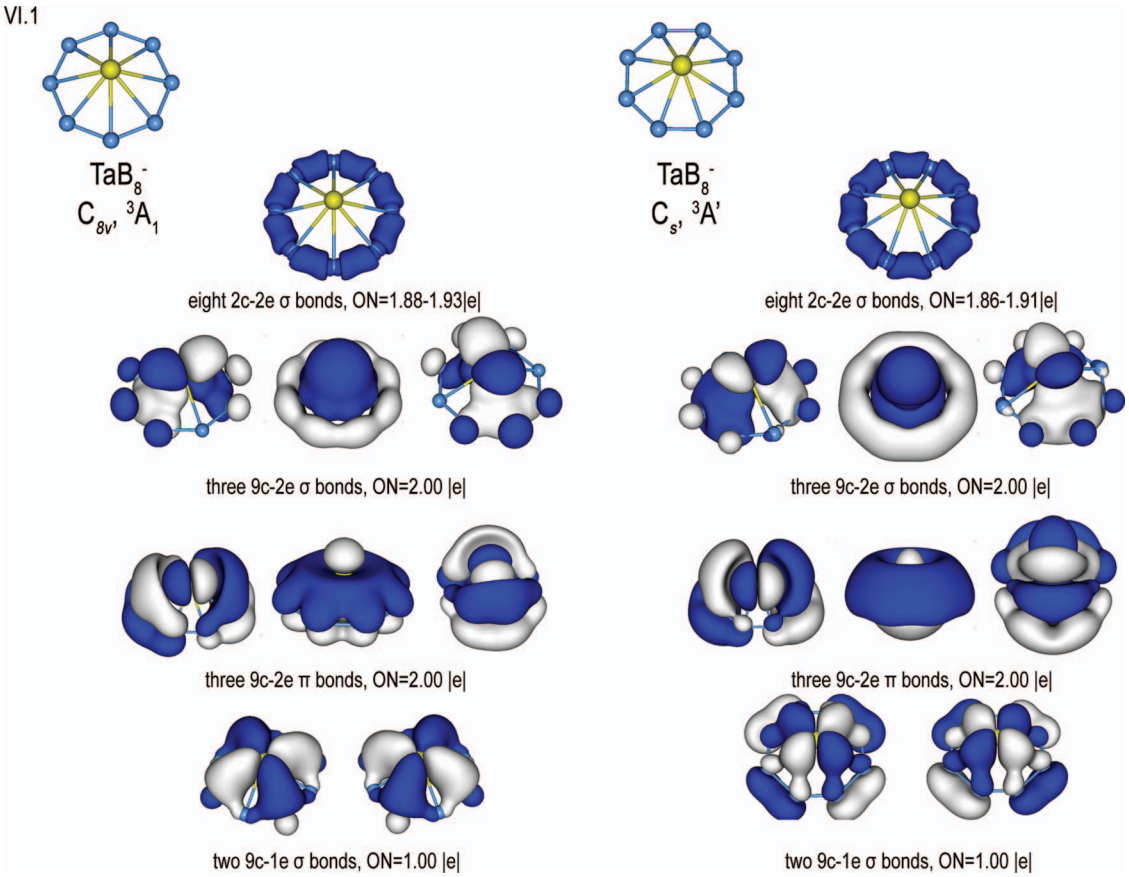


FIG. 6. Results of AdNDP analyses for the $C_{8v}$ and $C_s$ $TaB_8^-$.

This article is copyrighted as indicated in the article. Reuse of AIP content is subject to the terms at: http://scitation.aip.org/termsconditions. Downloaded to IP: 128.148.231.12 On: Mon, 26 May 2014 19:59:40

because of the $\pi$ antiaromaticity the Al atom is slightly bent out of plane in $AlB_6^-$. Thus, Ta can be considered as a better substitute of the peripheral B atom in the $B_7^-$ cluster to yield the doubly aromatic and perfectly planar $TaB_6^-$ cluster. This favourable bonding situation is why the fan structure of $TaB_6^-$ is not competitive.

The 3D global minimum structure of $TaB_7^-$ has seven localized 2c-2e $\sigma$ bonds (ON = 1.77-1.94 |e|), two delocalized 3c-2e $\sigma$ bonds (ON = 1.85 |e|), one delocalized 8c-2e $\sigma$ bond (ON = 1.99 |e|), three delocalized 8c-2e $\pi$ bonds (ON = 2.00 |e|), and one completely delocalized 8c-1e $\sigma$ bond (ON = 1.00 |e|) (Figure 5, V.1). The bonding pattern in this case is complicated and cannot be expressed in a simple manner. The term $\sigma$ and $\pi$ bonds are used loosely here. Clearly, the interactions between Ta and the boron atoms are optimized in the $TaB_7^-$ global minimum structure.

### C. $TaB_8^-$: On the way to Ta©$B_{10}^-$

Our calculations at different levels of theory found the pyramidal structure VI.1 to be the global minimum for $TaB_8^-$ (Figure 3(b)). As mentioned above, the structure VI.1 has $C_s$ point group symmetry at PBE0 level of theory and $C_{8v}$ symmetry at the PW91PW91 and M06-2x levels of theory. However, regardless of $C_s$ or $C_{8v}$ symmetry, our AdNDP analysis recovered similar chemical bonding patterns for both structures (Figure 6), because the structural distortion in the $C_s$ symmetry is very small.

While the $TaB_8^-$ cluster is not planar, the deviation from planarity is not that large in order to interpret its bonding approximately in terms of $\sigma$ and $\pi$ bonds. The AdNDP analysis showed eight localized 2c-2e $\sigma$ bonds (ON = 1.88-1.93 |e|) for the $B_8$ ring, three delocalized 9c-2e $\sigma$ bonds (ON = 2.00 |e|), three delocalized 9c-2e $\pi$ bonds (ON = 2.00 |e|), and two delocalized 9c-1e $\sigma$ bonds (ON = 1.00 |e|) (Figure 6, VI.1). The delocalized bonds closely resemble the canonical molecular orbitals. Thus, $TaB_8^-$ is $\pi$ aromatic with 6 $\pi$ electrons. Because the ground state of $TaB_8^-$ is open shell, the eight totally delocalized $\sigma$ electrons occupy five MOs, rendering it $\sigma$-aromatic. Thus, $TaB_8^-$ is doubly aromatic. The bonding of the triply $TaB_8^-$ is consistent with the design principle for metal-centred aromatic wheel-type clusters.[32–35] Clearly the $B_8$ ring is too small to fit the Ta atom, resulting in the pyramidal structure. We showed recently even the $B_9$ ring is not large enough to host a Ta atom, resulting a slight pyramidal distortion in $TaB_9^-$.[38] Only the $B_{10}$ ring is large enough for the Ta atom, resulting in the perfectly planar Ta©$B_{10}^-$ highest coordination borometallic molecular wheel. Thus, $TaB_8^-$ is on the way to the Ta©$B_{10}^-$ cluster by successive additions of two boron atoms.

## VII. CONCLUSIONS

A comprehensive experimental and theoretical study is reported on the structures and bonding in a series of $TaB_n^-$ ($n$ = 3–8) clusters to elucidate the steps necessary to form the highest coordination Ta©$B_{10}^-$ molecular wheel. Photoelectron spectroscopy is combined with extensive global minimum searches to locate the most stable structures and low-lying isomers for each cluster. $TaB_3^-$, $TaB_4^-$, and $TaB_5^-$ are found to have fan-like global minimum structures, in which the Ta atom interacts with the terminal boron atoms strongly with multiple Ta–B bond characters, whereas Ta interacts with the middle boron atom(s) via delocalized bonding. Thus, these clusters can also be viewed as ring structures with Ta being part of the ring. The fan growth mode is interrupted at $TaB_6^-$, which is found to have a planar hexagonal wheel-type structure with Ta being on the periphery of the wheel and a central B atom. The chemical bonding in the $TaB_6^-$ cluster is found to be reminiscent of the $AlB_6^-$ cluster and $TaB_6^-$ can be viewed to be doubly aromatic. The $TaB_7^-$ cluster is a three-dimensional boat-like global minimum structure, which seems to maximize Ta–B interactions. The global minimum of the $TaB_8^-$ cluster is found to be an octagonal pyramidal structure with Ta being out of the cyclic octagonal ring by about 1.1 Å. The $B_8$ ring is apparently too small to host a Ta atom, but the $TaB_8^-$ cluster can be viewed as the precursor to the Ta©$B_{10}^-$ molecular wheel. Addition of one B atom will form the pyramidal $TaB_9^-$ cluster, in which the Ta atom is only slightly above the $B_9$ ring.[38] And finally the $B_{10}$ ring is perfect to host a Ta atom to form the doubly aromatic Ta©$B_{10}^-$ molecular wheel.[35] The current study shows that the competition between B−B interactions and Ta−B interactions determines the most stable structures of the $TaB_n^-$ clusters. The structural evolution of the $TaB_n^-$ clusters is not only important to understand the formation mechanisms for the highest known coordination number in planar species (Ta©$B_{10}^-$)[40] but also provides insights into the interactions between early transition metals with boron.

## ACKNOWLEDGMENTS

This research was supported by the National Science Foundation (NSF) (CHE-1263745 to L.S.W. and CHE-1057746 to A.I.B.). Computer storage and other resources from the Division of Research Computing in the Office of Research and Graduate Studies at the Utah State University and an allocation of computer time from the Center for High Performance Computing at the University of Utah are gratefully acknowledged. A.I.B. greatly appreciates the funding from the J. W. Fulbright Commission for his work at Comenius University in Bratislava, Slovak Republic. I.Č. is thankful for support from the Slovak Research and Development Agency (Contract Nos. APVV-0059-10 and LPP-150-09). Part of this publication is the result of the project implementation "Amplification of the Center of Excellence on Green Chemistry Methods and Processes (CEGreenII)," ITMS 26240120025, supported by the Research & Development Operational Program funded by the ERDF.

[1] H. J. Zhai, L. S. Wang, A. N. Alexandrova, and A. I. Boldyrev, J. Chem. Phys. **117**, 7917 (2002).
[2] H. J. Zhai, A. N. Alexandrova, K. A. Birch, A. I. Boldyrev, and L. S. Wang, Angew. Chem., Int. Ed. **42**, 6004 (2003).
[3] H. J. Zhai, B. Kiran, J. Li, and L. S. Wang, Nat. Mater. **2**, 827 (2003).
[4] H. J. Zhai, L. S. Wang, A. N. Alexandrova, A. I. Boldyrev, and V. G. Zakrzewski, J. Phys. Chem. A **107**, 9319 (2003).

This article is copyrighted as indicated in the article. Reuse of AIP content is subject to the terms at: http://scitation.aip.org/termsconditions. Downloaded to IP: 128.148.231.12 On: Mon, 26 May 2014 19:59:40

[5]A. N. Alexandrova, A. I. Boldyrev, H. J. Zhai, L. S. Wang, E. Steiner, and P. W. Fowler, J. Phys. Chem. A **107**, 1359 (2003).
[6]A. N. Alexandrova, A. I. Boldyrev, H. J. Zhai, and L. S. Wang, J. Phys. Chem. A **108**, 3509 (2004).
[7]B. Kiran, S. Bulusu, H. J. Zhai, S. Yoo, X. C. Zeng, and L. S. Wang, Proc. Natl. Acad. Sci. U.S.A. **102**, 961 (2005).
[8]A. P. Sergeeva, D. Y. Zubarev, H. J. Zhai, A. I. Boldyrev, and L. S. Wang, J. Am. Chem. Soc. **130**, 7244 (2008).
[9]W. Huang, A. P. Sergeeva, H. J. Zhai, B. B. Averkiev, L. S. Wang, and A. I. Boldyrev, Nat. Chem. **2**, 202 (2010).
[10]A. P. Sergeeva, B. B. Averkiev, H. J. Zhai, A. I. Boldyrev, and L. S. Wang, J. Chem. Phys. **134**, 224304 (2011).
[11]Z. A. Piazza, W. L. Li, C. Romanescu, A. P. Sergeeva, L. S. Wang, and A. I. Boldyrev, J. Chem. Phys. **136**, 104310 (2012).
[12]A. P. Sergeeva, Z. A. Piazza, C. Romanescu, W. L. Li, A. I. Boldyrev, and L. S. Wang, J. Am. Chem. Soc. **134**, 18065 (2012).
[13]T. B. Tai, N. M. Tam, and M. T. Nguyen, Chem. Phys. Lett. **530**, 71 (2012).
[14]F. Li, P. Jin, D. e. Jiang, L. Wang, S. B. Zhang, J. Zhao, and Z. Chen, J. Chem. Phys. **136**, 074302 (2012).
[15]E. Oger, N. R. M. Crawford, R. Kelting, P. Weis, M. M. Kappes, and R. Ahlrichs, Angew. Chem., Int. Ed. **46**, 8503 (2007).
[16]A. N. Alexandrova, A. I. Boldyrev, H. J. Zhai, and L. S. Wang, Coord. Chem. Rev. **250**, 2811 (2006).
[17]A. N. Alexandrova, H. J. Zhai, L. S. Wang, and A. I. Boldyrev, Inorg. Chem. **43**, 3552 (2004).
[18]P. W. Fowler and B. R. Gray, Inorg. Chem. **46**, 2892 (2007).
[19]D. Y. Zubarev and A. I. Boldyrev, Phys. Chem. Chem. Phys. **10**, 5207 (2008).
[20]B. B. Averkiev, L. M. Wang, W. Huang, L. S. Wang, and A. I. Boldyrev, Phys. Chem. Chem. Phys. **11**, 9840 (2009).
[21]K. Exner and P. v. R. Schleyer, Science **290**, 1937 (2000).
[22]Z. X. Wang and P. v. R. Schleyer, Science **292**, 2465 (2001).
[23]L. M. Wang, W. Huang, B. B. Averkiev, A. I. Boldyrev, and L. S. Wang, Angew. Chem., Int. Ed. **46**, 4550 (2007).
[24]B. B. Averkiev, D. Y. Zubarev, L. M. Wang, W. Huang, L. S. Wang, and A. I. Boldyrev, J. Am. Chem. Soc. **130**, 9248 (2008).
[25]T. R. Galeev, A. S. Ivanov, C. Romanescu, W. L. Li, K. V. Bozhenko, L. S. Wang, and A. I. Boldyrev, Phys. Chem. Chem. Phys. **13**, 8805 (2011).
[26]S. D. Li, C. Q. Miao, J. C. Guo, and G. M. Ren, J. Am. Chem. Soc. **126**, 16227 (2004).
[27]R. M. Minyaev, T. N. Gribanova, A. G. Starikov, and V. I. Minkin, Mendeleev Commun. **11**, 213 (2001); V. I. Minkin, R. M. Minyaev, and R. Hoffmann, Russ. Chem. Rev. **71**, 869 (2002).
[28]T. R. Galeev, C. Romanescu, W. L. Li, L. S. Wang, and A. I. Boldyrev, J. Chem. Phys. **135**, 104301 (2011).
[29]W. L. Li, C. Romanescu, T. R. Galeev, L. S. Wang, and A. I. Boldyrev, J. Phys. Chem. A **115**, 10391 (2011).
[30]C. Romanescu, A. P. Sergeeva, W. L. Li, A. I. Boldyrev, and L. S. Wang, J. Am. Chem. Soc. **133**, 8646 (2011).
[31]Q. Luo, Sci. China Ser. B: Chem. **51**, 607 (2008); Q. Y. Wu, Y. P. Tang, and X. H. Zhang, *ibid.* **52**, 288 (2009); K. Ito, Z. Pu, Q. S. Li, and P. v. R. Schleyer, Inorg. Chem. **47**, 10906 (2008); **48**, 10679 (2009).
[32]C. Romanescu, T. R. Galeev, W. L. Li, A. I. Boldyrev, and L. S. Wang, Angew. Chem., Int. Ed. **50**, 9334 (2011).
[33]C. Romanescu, T. R. Galeev, W. L. Li, A. I. Boldyrev, and L. S. Wang, Acc. Chem. Res. **46**, 350 (2013).
[34]C. Romanescu, T. R. Galeev, A. P. Sergeeva, W. L. Li, L. S. Wang, and A. I. Boldyrev, J. Organomet. Chem. **721–722**, 148 (2012).
[35]T. R. Galeev, C. Romanescu, W. L. Li, L. S. Wang, and A. I. Boldyrev, Angew. Chem., Int. Ed. **51**, 2101 (2012).
[36]W. L. Li, C. Romanescu, T. R. Galeev, Z. A. Piazza, A. I. Boldyrev, and L. S. Wang, J. Am. Chem. Soc. **134**, 165 (2012).
[37]W. L. Li, C. Romanescu, Z. A. Piazza, and L. S. Wang, Phys. Chem. Chem. Phys. **14**, 13663 (2012).
[38]C. Romanescu, T. R. Galeev, W. L. Li, A. I. Boldyrev, and L. S. Wang, J. Chem. Phys. **138**, 134315 (2013).
[39]Y. Liao, C. L. Cruz, P. v. R. Schleyer, and Z. Chen, Phys. Chem. Chem. Phys. **14**, 14898 (2012).
[40]T. Heine and G. Merino, Angew. Chem., Int. Ed. **51**, 4275 (2012).
[41]I. Boustani and R. Pandey, Solid State Sciences **14**, 1591 (2012).
[42]L. Xie, W. L. Li, C. Romanescu, X. Huang, and L. S. Wang, J. Chem. Phys. **138**, 034308 (2013).
[43]L. S. Wang, H. S. Cheng, and J. W. Fan, J. Chem. Phys. **102**, 9480 (1995); L. S. Wang and X. Li, *In Advances in Metal and Semiconductor Clusters*, edited by M. A. Duncan (JAI, Greenwich, CT, 1998), Vol. 4, pp. 299–343.
[44]C. Adamo and V. Barone, J. Chem. Phys. **110**, 6158 (1999).
[45]J. P. Perdew, K. Burke, and M. Ernzerhof, Phys. Rev. Lett. **77**, 3865 (1996).
[46]P. J. Hay and W. R. Wadt, J. Chem. Phys. **82**, 270 (1985).
[47]R. A. Kendall, T. H. Dunning, Jr., and R. J. Harrison, J. Chem. Phys. **96**, 6796 (1992).
[48]T. H. Dunning, Jr., J. Chem. Phys. **90**, 1007 (1989).
[49]A. Bergner, M. Dolg, W. Kuechle, H. Stoll, and H. Preuss, Mol. Phys. **80**, 1431 (1993).
[50]M. Kaupp, P. v. R. Schleyer, H. Stoll, and H. Preuss, J. Chem. Phys. **94**, 1360 (1991).
[51]M. Dolg, H. Stoll, H. Preuss, and R. M. Pitzer, J. Phys. Chem. **97**, 5852 (1993).
[52]M. J. Frisch, G. W. Trucks, H. B. Schlegel *et al.*, GAUSSIAN09, Revision B.01, Gaussian, Inc, Wallingford, CT, 2009.
[53]U. Varetto, Molekel 5.4.0.8, Swiss National Supercomputing Centre, Manno, Switzerland, 2009.
[54]See supplementary material at http://dx.doi.org/10.1063/1.4820401 for the geometric structures and relative energies (CCSD(T)/Ta/Stuttgart/B/aug-cc-pVTZ, PBE0/Ta/Stuttgart/B/aug-cc-pVTZ, all at PBE0/Ta/Stuttgart/B/aug-cc-pVTZ optimized geometries) of all studied isomers. Cartesian coordinates of global minimum structures (PBE0/Ta/Stuttgart/B/aug-cc-pVTZ) for all considered stoichiometries.
[55]J. P. Perdew, J. A. Chevary, S. H. Vosko, K. A. Jackson, M. R. Pederson, D. J. Singh, and C. Fiolhais, Phys. Rev. B **46**, 6671 (1992).
[56]Y. Zhao and D. G. Truhlar, Theor. Chem. Acc. **120**, 215 (2008).

This article is copyrighted as indicated in the article. Reuse of AIP content is subject to the terms at: http://scitation.aip.org/termsconditions. Downloaded to IP: 128.148.231.12 On: Mon, 26 May 2014 19:59:40